Mechanical Systems and Signal Processing 143 (2020) 106842

Contents lists available at ScienceDirect

Mechanical Systems and Signal Processing

journal homepage: www.elsevier.com/locate/ymssp

Some practical regards on the application of the harmonic balance method for hysteresis models

Luccas Pereira Miguel [a], Rafael de Oliveira Teloli [a,*], Samuel da Silva [a]

[a] UNESP – Universidade Estadual Paulista, Faculdade de Engenharia de Ilha Solteira, Departamento de Engenharia Mecânica, Av. Brasil, 56, Ilha Solteira, 15385-000 SP, Brazil

ARTICLE INFO

Article history:
Received 25 February 2019
Received in revised form 8 August 2019
Accepted 21 March 2020
Available online 6 April 2020

Keywords:
Harmonic balance method
Hysteresis
Non-smooth dynamic systems
Bouc-Wen oscillator
LuGre model

ABSTRACT

Describing hysteretic systems with a closed-form solution is a challenging task due to some pitfalls regarding the non-smooth and memory effect mechanisms that do not permit, for example, to apply conventional frequency domain methods. Consequently, it is necessary to use some previous smoothing scheme to approximate the hysteresis loop. Thus, this work proposes a new way for approximating the hysteresis loops analytically using a truncated Taylor series as a simple and effective smoothing procedure to enable the use of the harmonic balance method. Two benchmark hysteretic systems, which were not addressed yet by closed-form solutions obtained by the harmonic balance method, are simulated to demonstrate the benefits of the proposed strategy. The first one is a Bouc-Wen oscillator and the second one is a LuGre model. The comparison with numerical integrations and other literature methods have shown that the obtained analytical solutions of the suggested smoothed hysteresis loops are adequate to describe the fundamental dynamics in both models using a feasible frequency domain approximation.

1. Introduction

Engineering systems generally have assembled structures with bolted and viscoelastic joints [1,2], damping devices to mitigate excessive vibrations [3,4] or even materials that experiment variabilities on their properties according to the operational conditions [5]. A typical feature of these applications is that they may exhibit nonlinearities in their damping source due to the hysteresis effect. This hysteresis arises from the nonlinear interaction of three variables named as input, output and an evolutionary variable that induces a delay and memory dependency among them [6]. The interaction occurs from different mechanisms and therefore there exist many phenomenological and empirical models accessible in the literature for explaining hysteretic features, as non-smoothness, multiple solutions, and rate-dependent or rate-independent memory effects.

The classical Bouc-Wen model [7,8] plays a vital role among the different models used to describe hysteresis due to its versatility in modeling a wide range of loops from real systems. Additionally, the proposal of closed-form solutions has begun to gain space because of its adequate applicability for parametric calibration, identification purposes and system designing [9]. Shen et al. (2005) [10] proposed a comparative analysis between both the equivalent linearization method and the averaging method, which were used to obtain analytical expressions of a magnetorheological damper in steady-state regime. The methods achieved a close approximation with experimental data and, besides, they provided an attractive

* Corresponding author.
E-mail addresses: luccas.miguel@unesp.br (L.P. Miguel), rafael.teloli@unesp.br (R.d.O. Teloli), samuel.silva13@unesp.br (S. da Silva).

https://doi.org/10.1016/j.ymssp.2020.106842
0888-3270/

physical acumen about how the variations on modeling parameters of the damper device could affect both the responses curves and the hysteresis loop, which is an advantage of the white-box modeling. Laxalde et al. (2006) [11] examined the usefulness of a nonlinear hysteretic absorber described by a Bouc-Wen model, which was used as a dissipation source of the vibratory energy. The periodic solutions predicted by the averaging strategy open the possibility of establishing some designing criteria to optimize the process of energy dissipation. Various works have already proposed analytical solutions of the Bouc-Wen oscillator, for example in [12,13].

Nevertheless, the friction-induced hysteresis originated from the relative motion between contact surfaces is also essential for engineering purposes. Many of the friction features, as memory-dependency, friction force as a function of velocity, the stick–slip dynamics, and the Stribeck effect, can be observed in tribology [14], mechanical joints [15,16], servo machines [17] and so on [18]. Another model used is the LuGre model [19]. This model is an attractive alternative to capture the friction features with the advantage of taking into account the Stribeck effect, which is beneficial to explain the stick–slip motion accurately [20]. However, as pointed by Huang et al. (2018) [21], leading the steady-state response of frictional models by numerical integration is, in general, an arduous task due to the significant computational cost required to calculate the desired response until the transient state vanishes. In this way, the proposing of determining closed-form solutions to avoid that technical issue seems to be a welcome strategy, and regarding the LuGre model, only a couple of works have been proposed [22,23].

Variants of the harmonic balance method, such as the fast Galerkin method applied on the Bouc-Wen model [24,25] and the incremental harmonic balance to solve the LuGre model [26], were used successfully, once no laborious mathematical manipulation was required. In this way, another alternative which may be used to deal with frictional motion described by the Bouc-Wen and LuGre model is the alternating frequency-time (AFT) method, developed by [27] and successfully implemented for application in turbomachinery blading with friction interfaces [28].

Indeed, the non-smoothness of both differential models establish a restrictive condition in forming the balance equations, because it does not permit the explicit expansion of hysteretic forces in terms of the displacement. Also, it is important to point out that, although this paper address only the Bouc-Wen and the LuGre models, deriving analytical approximations for other hysteretic systems through the harmonic balance method cannot be performed directly. Consequently, a smoothing procedure should be performed on the hysteretic systems before deriving the analytical solutions by the harmonic balance technique. Thus, the present paper proposes to introduce closed-form solutions for the Bouc-Wen and LuGre models assuming a smoothing procedure and then to apply the harmonic balance.

The complete smoothing procedure applied here initially consists of approximating the hysteretic restoring force by piecewise nonlinear expressions and then to expand them as explicit functions of displacement by the Taylor series approach, which covers the idea for using the harmonic balance method. Although both models manifest hysteresis in the input–output map, each one of them has particularities. For example, the hysteresis loop of the Bouc-Wen model can be broken into four different intervals on the force $\times$ displacement plane, admitting to rewrite the restoring force equations by using the Taylor series approach. On another hand, in the motion equation of the LuGre model does not accept a similar procedure. Instead of dealing directly with the LuGre motion equation, this paper employs the loading–unloading restoring force expressions obtained analytically by Naser and Ikhouane (2016) [22] as starting point for the smoothing procedure and, at last, it aims to apply the Taylor series on these equations. Although the precise expressions derived here are only useful when the hysteresis is weak, the simplicity in applying the harmonic balance method alongside the Taylor series provides interesting white-box modeling of hysteretic systems, in addition to the fact that, to our knowledge, similar results were not illustrated in the previous papers.

The outline of this paper is organized as follows. First of all, Section 2 shows the background to smooth the Bouc-Wen and LuGre models. The harmonic balance method and the particularities involving its application in hysteretic systems are formulated in Section 3. Next, Section 4 provides numerical applications with the Bouc-Wen and LuGre models to address the applicability of the proposed method in obtaining analytical solutions through the frequency domain method for both hysteretic systems. Finally, the final remarks of the entire work, as well as future research, are highlighted in Section 5.

2. Smoothing of hysteresis

Methods for obtaining approximate solutions are often a quite useful alternative when an explicit solution demands arduous algebraic manipulations or even it does not exist. Nevertheless, these methods cannot be applied directly to evaluate, for example, the Bouc-Wen and LuGre models, given that both hysteretic restoring forces cannot be expressed as an explicit function of the displacement or velocity. In this context, smoothing procedures have become increasingly important to extend analytical approaches to deal not only with hysteretic systems but also systems with complicated nonlinear stiffness [29]. Thus, this Section reports in details the smoothing procedure implemented here to the Bouc-Wen and LuGre models.

2.1. Smoothing of the Bouc-Wen model

The so-called Bouc-Wen model used to describe a single-degree-of-freedom system with rate-independent hysteresis is given by [7,8]:

$$m\ddot{y}(t) + c\dot{y}(t) + ky(t) + \mathcal{Z}(y,\dot{y}) = u(t) \tag{1}$$

$$\dot{\mathcal{Z}}(y,\dot{y}) = \alpha\dot{y}(t) - \beta\Big(\gamma|\dot{y}(t)||\mathcal{Z}(y,\dot{y})|^{\nu-1}\mathcal{Z}(y,\dot{y}) + \delta\dot{y}(t)|\mathcal{Z}(y,\dot{y})|^{\nu}\Big) \tag{2}$$

where $y, \dot{y}$ and $\ddot{y}$ denote the displacement [m], velocity [m/s] and acceleration [m/s^2)], respectively, for an excitation input u [N]. Regarding the model parameters, m [kg] is the mass constant, c [Ns/m] is the viscous damping, k [N/m] is the linear stiffness. The term $\mathcal{Z}$, which encodes the hysteretic restoring force, obeys the first-order differential equation of $\dot{\mathcal{Z}}$, whereas β, α [N/m], γ [m^{-1}], δ [m^{-1}] and ν control the shape of the hysteresis loop and are known as the Bouc-Wen parameters. Also, this paper considers the specific case of $\nu = 1$. As pointed by [30], the term $\mathcal{Z}(y,\dot{y})$ does not offer an explicit expansion as a function of y and $\dot{y}$, which restricts the applicability of the harmonic balance technique or even another white-box method.

Fig. 1(a) illustrates the hysteresis loop exhibited by a Bouc-Wen oscillator in the restoring force $\times$ displacement plane. Many features of the system with hysteresis are displayed in Fig. 1, for instance, the hysteretic force is a multi-valued function due to the presence of memory dependency, since $\mathcal{Z}(y,\dot{y})$depends not only on the instantaneous output y but also on the history of all previous outputs. Further, one of the main characteristics of the Bouc-Wen oscillator lies on the possibility of transforming the non-smooth hysteretic force into an equivalent piecewise smooth problem dividing the total hysteretic restoring force into four different components, named as $\mathcal{Z}_1, \mathcal{Z}_2, \mathcal{Z}_3$ and $\mathcal{Z}_4$ regarding the paths AC, CD, DB and BA, respectively, from the enclosed area $ACDB$. The switches between the force components occur at a time interval of $\frac{\pi}{2\omega}$ when a bounded harmonic input, defined in a period $T \in [0\,\frac{2\pi}{\omega}]$, is applied, where ω [rad/s] is the excitation frequency. Fig. 1(b) depicts the exemplifying hysteretic output y from Fig. 1(a).

Dividing the Eq. (2) by $\dot{y}$ and rearranging terms yields:

$$\frac{d\mathcal{Z}}{dy} = \alpha - \beta|\mathcal{Z}|[\mathrm{sgn}(\dot{y}\mathcal{Z})\gamma + \delta] \tag{3}$$

Eq. (3) provides an attractive feature about the slope and shape of the hysteresis loop. For instance, α controls the slope of the restoring force, and it is associated with the linear stiffness k, appearing in the resonance frequency at $\omega_n = \sqrt{(k+\alpha)m^{-1}}$, whereas if β is null, then the restoring force is linear. Also, $\gamma > 0$ is responsible for the multiple solutions of the hysteresis loop, creating the paths DBA and ACD, so-called as loading and unloading regimes of the restoring force, respectively. Notwithstanding, the possibilities of combining $\pm\gamma + \delta$ produce the hardening or softening characteristics of the hysteresis loop.

The defined integral of Eq. (3), which depends upon the signs assumed by $\dot{y}$ and $\mathcal{Z}$, divides the hysteresis loop into four different paths:

- path (i): $\dot{y} \leqslant 0, \mathcal{Z} \geqslant 0$

$$\mathcal{Z}_1 = \frac{\alpha}{\beta(\delta-\gamma)}\left(1 - e^{-\beta(\delta-\gamma)(y-y_0)}\right) \tag{4}$$

- path (ii): $\dot{y} \leqslant 0, \mathcal{Z} \leqslant 0$

$$\mathcal{Z}_2 = -\frac{\alpha}{\beta(\delta+\gamma)}\left(1 - e^{\beta(\delta+\gamma)(y-y_0)}\right) \tag{5}$$

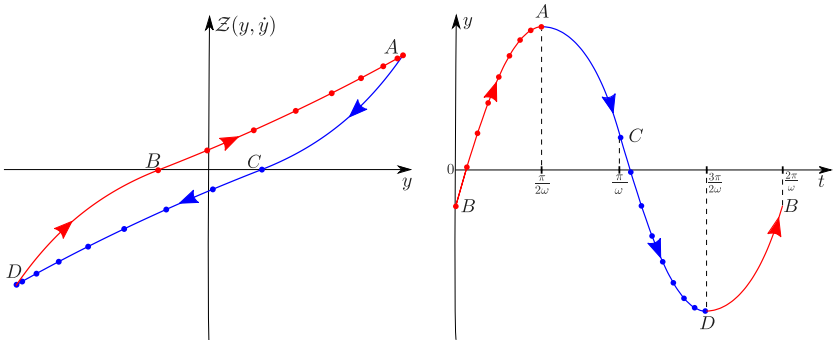

(a) Hysteresis loop of the Bouc-Wen model

(b) Exemplifying hysteretic output.

Fig. 1. Illustrative example of the hysteresis loop of a Bouc-Wen model. — represents the path described by $\mathcal{Z}_1$, ● is for $\mathcal{Z}_2$, — represents $\mathcal{Z}_3$ and ● is $\mathcal{Z}_4$.

- path (iii): $\dot{y} \geqslant 0, \mathcal{Z} \leqslant 0$

$$\mathcal{Z}_3 = -\frac{\alpha}{\beta(\delta-\gamma)}\left(1 - e^{\beta(\delta-\gamma)(y+y_0)}\right) \tag{6}$$

- path (iv): $\dot{y} \geqslant 0, \mathcal{Z} \geqslant 0$

$$\mathcal{Z}_4 = \frac{\alpha}{\beta(\delta+\gamma)}\left(1 - e^{-\beta(\delta+\gamma)(y+y_0)}\right) \tag{7}$$

where the paths (iii) and (iv), with $\dot{y} \geqslant 0$, compose the loading regime of the hysteresis loop, whereas the paths (i) and (ii), with $\dot{y} \leqslant 0$, are the unloading one, and in addition, since the paths start at $\mathcal{Z} = 0$, then y_0 is called as threshold displacement and corresponds to the points B and C in Fig. 1. Moreover, the transition between each restoring force path is continuous, exemplifying $\mathcal{Z}_4\left(y\left(\frac{\pi}{2\omega}\right), \dot{y}\left(\frac{\pi}{2\omega}\right)\right) = \mathcal{Z}_1\left(y\left(\frac{\pi}{2\omega}\right), \dot{y}\left(\frac{\pi}{2\omega}\right)\right)$ where this continuity relation is valid on all time interval, and the hysteresis loop is symmetric in relation to the coordinate $\left(\frac{y_{\max}+y_{\min}}{2}, 0\right)$ on the y and $\mathcal{Z}$ axes, respectively. Therefore, the piecewise functions that represent the hysteresis loop allows the expansion into finite terms of the Taylor series approach around y_0:

$$\mathcal{Z}_1 \approx \frac{\alpha}{\beta(\delta-\gamma)}\left(1 - \left[\sum_{n=0}^{\infty}\frac{[-\beta(\delta-\gamma)]^n(y-y_0)^n}{n!}\right]\right) \tag{8}$$

$$\mathcal{Z}_2 \approx -\frac{\alpha}{\beta(\delta+\gamma)}\left(1 - \left[\sum_{n=0}^{\infty}\frac{[\beta(\delta+\gamma)]^n(y-y_0)^n}{n!}\right]\right) \tag{9}$$

$$\mathcal{Z}_3 \approx -\frac{\alpha}{\beta(\delta-\gamma)}\left(1 - \left[\sum_{n=0}^{\infty}\frac{[\beta(\delta-\gamma)]^n(y+y_0)^n}{n!}\right]\right) \tag{10}$$

$$\mathcal{Z}_4 \approx \frac{\alpha}{\beta(\delta+\gamma)}\left(1 - \left[\sum_{n=0}^{\infty}\frac{[-\beta(\delta+\gamma)]^n(y+y_0)^n}{n!}\right]\right) \tag{11}$$

Therefore, the piecewise functions (8)–(11) are rewritten as a smooth polynomial function of the displacement of y, rendering it possible to apply the harmonic balance method. The method is executed admitting a combination of the paths regarding their valid time interval. Although there exist other available methods to approach the piecewise restoring forces through polynomial functions, the Taylor series provides the required condition for expanding the polynomial coefficients as a function of the physical parameters and, in addition, the series guarantees satisfying results using only a few terms, as will be addressed in Section 4.

2.2. Smoothing of the LuGre model

The LuGre model [19] was proposed initially to describe limit cycles that occur due to the presence of friction in control applications [31]. The friction effect has an abrupt transition between the stick–slip states, which evidences the non-smoothness in the nonlinear restoring force, as other hysteretic systems. The model equation is given by:

$$m\ddot{y}(t) + ky(t) + \mathcal{Z}(\dot{y}) = u(t) \tag{12}$$

where the term $\mathcal{Z}(\dot{y})$ [N] is the hysteretic restoring force of the LuGre model and obeys the following relation:

$$\mathcal{Z}(\dot{y}) = \sigma_0 \upsilon(\dot{y}) + \sigma_1 \dot{\upsilon}(\dot{y}) + c\dot{y}(t) \tag{13}$$

where c [Ns/m] is the linear damping, σ_0 [N/m] and σ_1 [Ns/m] denote the microstiffness and microdamping coefficients, respectively. The terms $\upsilon(\dot{y})$ [m] and $\dot{\upsilon}(\dot{y})$ [m/s] are microdisplacement and velocity, respectively, where the latter follows the nonlinear differential equation:

$$\dot{\upsilon}(\dot{y}) = \dot{y}(t) - \sigma_0 \frac{|\dot{y}(t)|}{\mathcal{G}(\dot{y})}\upsilon(\dot{y}) \tag{14}$$

The model is an enhancement of the Dahl model [32], since it is suitable to achieve effects which depend on the velocity magnitude [33]. These effects can be achieved by the term $\mathcal{G}(\dot{y})$ written as:

$$\mathcal{G}(\dot{y}) = \mathcal{F}_c + (\mathcal{F}_s - \mathcal{F}_c)\exp\left(-\left[\frac{\dot{y}(t)}{V_s}\right]^2\right) \tag{15}$$

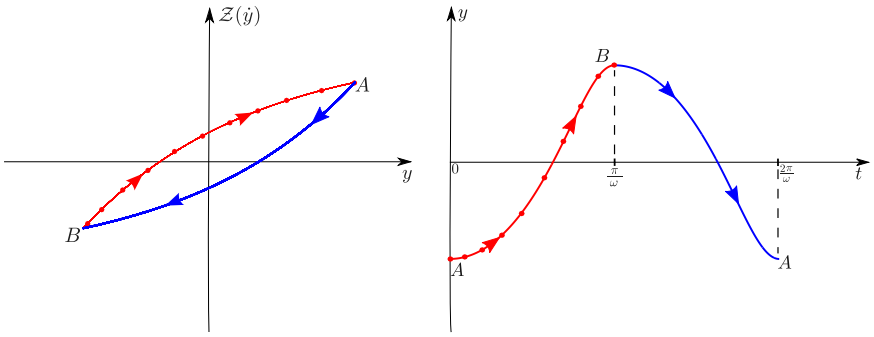

(a) Hysteresis Loop pf the LuGre model (b) Hysteretic output

Fig. 2. Loading and unloading regimes exemplified on the hysteresis loop. —, the unloading regime, whereas — • — is the loading one.

where $\mathcal{F}_c$ [N] and $\mathcal{F}_s$ [N] are the friction parameters, and V_s [m/s] is the switching velocity related to change of the nonlinear restoring force, and known as the Stribeck velocity.

Fig. 2(a) illustrates the steady-state hysteresis loop generated by the LuGre model. As the Bouc-Wen model, the hysteretic force is also a multi-valued function with memory dependency. Further, the figure depicts two different paths on the restoring force $\times$ displacement plane, which is known as loading and unloading regimes of the hysteresis loop. The switch between these regimes occurs according to the sign of the velocity, in that if $\text{sign}[\dot{y}(t)] > 0$, then the hysteretic force is on the loading regime. Otherwise, the hysteretic force is on the unloading regime. As seen in Fig. 2(b), which illustrates the output $y(t)$ from the hysteresis loop in Fig. 2(a), the switch between the regimes occurs at a time interval of $\frac{\pi}{\omega}$ when subjected to a bounded harmonic input fixed in a period $T \in [0\,\frac{2\pi}{\omega}]$, where ω is the excitation frequency.

The application of the harmonic balance method on the LuGre model exhibits challenging issues. For example, regarding the multi-valued hysteretic force, one observes two different regimes of motion depend on the term $\dot{v}(\dot{y})$, which cannot be written as an explicit function of $\dot{y}$. A smoothing procedure on the LuGre restoring force used here is based on the equations derived by Naser and Ikhouane (2015) [22]. These equations were obtained after employing the concepts of consistency and strong consistency in the LuGre motion equation. These equations split the hysteretic force into two smooth functions of $y(t)$ given by:

$$\mathcal{Z}_{\uparrow}(y) = \varrho\left[1 - \lambda e^{-\frac{\sigma_0}{\varrho}(y - y_{\min})}\right] + \sigma_2 \dot{y}_{\text{ini}} \tag{16}$$

$$\mathcal{Z}_{\downarrow}(y) = \varrho\left[\lambda e^{-\frac{\sigma_0}{\varrho}(y_{\max} - y)} - 1\right] + \sigma_2 \dot{y}_{\text{ini}} \tag{17}$$

where $\mathcal{Z}_{\uparrow}(y)$ [N] is the loading regime and $\mathcal{Z}_{\downarrow}(y)$ [N] is the unloading regime, such that when combined, they form the hysteresis loop. Besides, $y_{\max}$ and $y_{\min}$ are the maximum and minimum steady-state displacements, respectively, $\dot{y}_{\text{ini}}$ is the initial velocity, ϱ is the initial value of the function $\mathcal{G}(\dot{y}(t=0))$ and λ is described as:

$$\lambda = \frac{2}{1 + e^{\frac{\sigma_0(y_{\min} - y_{\max})}{\varrho}}} \tag{18}$$

Although the Eqs. 16,17 are smooth, they are a couple of transcendental equations with a significant difficulty level to approach by the Fourier analysis. Hence, an expansion by Taylor series around $y = 0$ is suggested, which is the symmetry point between the maximum and minimum displacement outputs at the steady-state regime. Thus, the functions $\mathcal{Z}_{\uparrow}(y)$ and $\mathcal{Z}_{\downarrow}(y)$ can be written as:

$$\mathcal{Z}_{\uparrow}(y) \approx \varrho\left(1 - \lambda\left(\sum_{n=0}^{\infty} \frac{e^{\frac{\sigma_0 y_{\min}}{\varrho}} \sigma_0^n y^n(t)(-1)^n}{n!\varrho^n}\right)\right) + \sigma_2 \dot{y}_{\text{ini}} \tag{19}$$

$$\mathcal{Z}_{\downarrow}(y) \approx \varrho\left(\lambda\left(\sum_{n=0}^{\infty} \frac{e^{-\frac{\sigma_0 y_{\max}}{\varrho}} \sigma_0^n y^n(t)}{n!\varrho^n}\right) - 1\right) + \sigma_2 \dot{y}_{\text{ini}} \tag{20}$$

With the loading and unloading forces rewritten as polynomial functions that depend explicitly on $y(t)$, the main pitfalls associated with the application of the harmonic balance are solved, remaining only mathematical adaptations of the method to the piecewise smooth cases, which are presented after this. Also, the expressions proposed by Naser and Ikhouane (2015) [22] are valid only for quasi-static forcing conditions.

3. Harmonic balance method

There are different alternatives to approximate the output of nonlinear systems by analytical descriptions, e.g., by decomposing the total response into linear and nonlinear components [34,35], or even using the class of perturbation methods [36]. When a mono–harmonic input is applied to a nonlinear system, usually, due to the presence of higher-order harmonics as a result of existing nonlinearities, its response exhibits waveform distortions. Thus, the fundamental premise of the harmonic balance method is to represent the system response through the Fourier series, decomposing the higher-order harmonic components as a sum of sines and cosines. In this context, the harmonic balance method is utilized to derive the closed-form solutions for the solution of hysteretic systems after employing the Taylor series approach as smoothing procedure of the hysteretic restoring forces. To achieve this, some assumptions demand to be done. Indeed, the harmonic balance method provides an adequate framework to deal with strong nonlinearities, e. g. [37], but in this work scenario, the method is valid for forcing conditions which guarantees a weak hysteresis force or, in other words, for forcing conditions in which the system output admits an approximation by the Fourier series. Further, the implementation scheme of the harmonic balance for hysteretic systems has particularities that are explained throughout this section since the analysis by Fourier series requires to analyze the piecewise expressions of the hysteretic restoring force.

3.1. General harmonic balance

The system analyzed here to exemplify the harmonic balance method is the symmetric Duffing oscillator with a smooth stiffness nonlinearity [38]:

$$m\ddot{y}(t) + c\dot{y}(t) + ky(t) + \underbrace{k_3 y^3(t)}_{=\mathcal{F}_{nl}(y)} = u(t) \tag{21}$$

where $\mathcal{F}_{nl}(y)$ [N] is the nonlinear restoring force. The trial solution of the nonlinear system when subjected to a harmonic input $u(t) = A\sin(\omega t)$ is assumed to be written as a Fourier series:

$$y(t) = a_0 + \sum_{n=1}^{\kappa}[a_n \cos(n\omega t) + b_n \sin(n\omega t)] \tag{22}$$

where a_n and b_n are the coefficients of the series and κ corresponds to the number of harmonics considered to approach the desired solution. After substituting the series of $y(t)$ in the motion Eq. (21), the nonlinear restoring force is also formulated as the Fourier series:

$$\mathcal{F}_{nl}(y) = \frac{\mathcal{A}_0}{2} + \sum_{n=1}^{\kappa}[\mathcal{A}_n \cos(n\omega t) + \mathcal{B}_n \sin(n\omega t)] \tag{23}$$

where $\mathcal{A}_n$ and $\mathcal{B}_n$ are the coefficients of the series of the restoring force. As the term $\mathcal{F}_{nl}(y)$ is continuous over all the oscillation period established in $[0, \frac{2\pi}{\omega}]$, the classical Fourier analysis can properly expand it [39–42]:

$$\mathcal{A}_n = \frac{\omega}{\pi}\int_0^{\frac{2\pi}{\omega}} \mathcal{F}_{nl}(t)\cos(n\omega t)dt \tag{24}$$

$$\mathcal{B}_n = \frac{\omega}{\pi}\int_0^{\frac{2\pi}{\omega}} \mathcal{F}_{nl}(t)\sin(n\omega t)dt \tag{25}$$

Substituting Eqs. (22)–(25) into the motion Eq. (21) yields:

$$\begin{aligned} A\sin(\omega t) = &-m\omega^2\left\{\sum_{n=1}^{\kappa} n^2[a_n\cos(n\omega t) + b_n\sin(n\omega t)]\right\} \\ &+c\omega\left\{\sum_{n=1}^{\kappa} n[-a_n\sin(n\omega t) + b_n\cos(n\omega t)]\right\} \\ &+k\left\{a_0 + \sum_{n=1}^{\kappa}[a_n\cos(n\omega t) + b_n\sin(n\omega t)]\right\} \\ &+\tfrac{\mathcal{A}_0}{2} + \sum_{n=1}^{\kappa}[\mathcal{A}_n\cos(n\omega t) + \mathcal{B}_n\sin(n\omega t)] \end{aligned} \tag{26}$$

Balancing the equal harmonic terms from Eq. (26) results in the following system of equations:

$$\begin{aligned}
&\underbrace{\sum_{n=1}^{\kappa}\left[-m(\omega n)^2 a_n + c(n\omega)b_n + ka_n + \mathcal{A}_n\right]}_{\text{cosine terms}} = 0\\
&\underbrace{-m(\omega)^2 b_1 - c\omega a_1 + b_1 k + \mathcal{B}_1]}_{\text{first order sine terms}} = A\\
&\underbrace{\sum_{n=2}^{\kappa}\left[-m(\omega n)^2 b_n - c(n\omega)a_n + kb_n + \mathcal{B}_n\right]}_{\text{sine terms}} = 0\\
&\underbrace{ka_0 + \frac{\mathcal{A}_0}{2}}_{\text{remaining terms}} = 0
\end{aligned} \tag{27}$$

Thus, it is demanded to solve all the series coefficients that minimize the set of equations in (27). There are constraints to handle this task, e. g., a particular frequency range where multiple solutions exist. Here, the Newton–Raphson method is utilized for solving Eq. (27).

3.2. Particularities of the harmonic balance method for hysteretic system

As discussed before, the method can be realized directly in a smooth nonlinear system since the restoring force is continuous on the oscillation period [43,44]. However, the piecewise smooth equations from both Bouc-Wen and LuGre models require modifications in the Fourier approach meaning to describe each restoring force term properly in its valid time intervals. In sum, the harmonic balance generates an average hysteretic restoring force based on splitting the coefficients of the series $\mathcal{A}$ and $\mathcal{B}$ according to the valid oscillation period of $\mathcal{Z}_1(y,\dot{y}), \mathcal{Z}_2(y,\dot{y}), \mathcal{Z}_3(y,\dot{y})$ and $\mathcal{Z}_4(y,\dot{y})$ for the Bouc-Wen model, and $\mathcal{Z}_{\uparrow}(y)$ and $\mathcal{Z}_{\downarrow}(y)$ for the LuGre model. The particularities involved in these both models are similar to the strategy required to deal with the Coulomb friction law, which decomposes the friction force into the stick and slip intervals [45].

3.2.1. Fourier analysis of the Bouc-Wen model

The hysteretic restoring force of the Bouc-Wen model was split into four motion intervals, where each of them is valid on a quarter of the total oscillation period, as exposed in Fig. 1. Then, the general expression of the average restoring force in steady-state is constituted as:

$$\mathcal{Z} = \sum_{n=1}^{\kappa}[\mathcal{A}_n \cos(n\omega t) + \mathcal{B}_n \sin(n\omega t)] \tag{28}$$

where the Fourier expansion of the coefficients is given by:

$$\mathcal{A}_n = \frac{\omega}{\pi}\left(\begin{array}{l}\int_0^{\frac{\pi}{2\omega}} \mathcal{Z}_1 \cos(n\omega t)dt + \int_{\frac{\pi}{2\omega}}^{\frac{\pi}{\omega}} \mathcal{Z}_2 \cos(n\omega t)dt + \\ \int_{\frac{\pi}{\omega}}^{\frac{3\pi}{2\omega}} \mathcal{Z}_3 \cos(n\omega t)dt + \int_{\frac{3\pi}{2\omega}}^{\frac{2\pi}{\omega}} \mathcal{Z}_4 \cos(n\omega t)dt\end{array}\right) \tag{29}$$

$$\mathcal{B}_n = \frac{\omega}{\pi}\left(\begin{array}{l}\int_0^{\frac{\pi}{2\omega}} \mathcal{Z}_1 \sin(n\omega t)dt + \int_{\frac{\pi}{2\omega}}^{\frac{\pi}{\omega}} \mathcal{Z}_2 \sin(n\omega t)dt + \\ \int_{\frac{\pi}{\omega}}^{\frac{3\pi}{2\omega}} \mathcal{Z}_3 \sin(n\omega t)dt + \int_{\frac{3\pi}{2\omega}}^{\frac{2\pi}{\omega}} \mathcal{Z}_4 \sin(n\omega t)dt\end{array}\right) \tag{30}$$

The Bouc-Wen hysteresis loop is symmetric regarding each regime of motion. Consequently, the Fourier terms related to asymmetric motion are null.

3.2.2. Fourier analysis of the LuGre model

Unlike the hysteretic restoring force of the Bouc-Wen model, the hysteresis loop of the LuGre model is classified into loading and unloading regimes, as observed in Fig. 2, whereas the switch between the regimes occurs at one-half of the total period. As the hysteresis loop of the model is symmetric in the steady-state regime, its general expression of the averaging restoring force is equal to Eq. (28), whereas its coefficients are provided by:

$$\mathcal{A}_n = \frac{\omega}{\pi}\left(\int_{-\frac{\pi}{2\omega}}^{\frac{\pi}{2\omega}} \mathcal{Z}_{\uparrow} \cos(n\omega t)dt + \int_{\frac{\pi}{2\omega}}^{\frac{3\pi}{2\omega}} \mathcal{Z}_{\downarrow} \cos(n\omega t)dt\right) \tag{31}$$

$$\mathcal{B}_n = \frac{\omega}{\pi}\left(\int_{-\frac{\pi}{2\omega}}^{\frac{\pi}{2\omega}} \mathcal{Z}_{\uparrow} \sin(n\omega t)dt + \int_{\frac{\pi}{2\omega}}^{\frac{3\pi}{2\omega}} \mathcal{Z}_{\downarrow} \sin(n\omega t)dt\right) \tag{32}$$

The equations presented here are valid for a generic case with harmonics of κ-order and n terms of Taylor series approach. It is remarkable that the more harmonics and terms are used to calculate the analytical solution, the higher the mathematical complexity to acquire the coefficients of the series will be. In contrast, since the hysteresis admitted in this work is weak, only a few terms are required to achieve adequate results. Next section illustrates the harmonic balance method implemented to two common benchmark hysteretic systems. Then, the analytical output and the one obtained by numerical integration are both examined. Finally, it was used the open source solver *wxMaxima*[1] to perform all the necessary algebraic manipulations.

4. Numerical application

The analysis of the harmonic balance to deal with hysteretic systems begins with the Bouc-Wen oscillator. The model parameters considered in this work were extracted from the benchmark recently proposed by Noël and Shoukens (2016) [46] at the Workshop on Nonlinear System Identification Benchmarks. The hysteretic benchmark was addressed with different identification strategies, for instance, the polynomial nonlinear state-space models [47,48], evolutionary optimization algorithms [49], stochastic subspace methods [50] and harmonic probing methods [51], but no attempts were handled with the harmonic balance method. First, a numerical analysis is executed to select carefully how many terms are required for expanding the Eqs. (8)–(11) into the Taylor series approach. Therefore, with the analytical representations of the piecewise functions well established, it is possible to calculate the coefficients of the series and to predict the output, as well as the hysteresis loop of the Bouc-Wen model by the harmonic balance method. The frequency response curve is also provided.

The LuGre model used here was first proposed as a benchmark by de Wit et al. (1995) [19] and since then it has been used for testing identification methods and to approximate experimental setups [52–54]. Although only a few white-box models of the LuGre oscillator exist in the literature, this work bridges the gap between analytical description through series approaching and non-smooth systems, providing a helpful alternative to analyze dynamic features of the friction effect under the steady-state regime of motion. As done for the Bouc-Wen case, to deal with the LuGre model it is essential to define the number of terms used into the Taylor series approach of Eqs. 19,20 and then obtain the coefficients of the series corresponding to the average restoring force by the Fourier analysis.

4.1. Numerical application for the Bouc-Wen model

The Bouc-Wen model parameters are displayed in Table 1. Before starting to derive analytical expressions for the coefficients of the series, some numerical simulations are handled to establish how many terms are required to expand the Eqs. (8)–(11) using the Taylor series approach.

The bar graph in Fig. 3 shows the normalized mean square error (NMSE) between the hysteresis loop approached by Taylor series expansion with regard the loop obtained through numerical integration of Eqs. 1,2 considering the 4$^{\text{th}}$ order Runge–Kutta method with variable time step. The NMSE is defined as:

$$\text{NMSE} = 100 \times \frac{||\mathcal{Z}(y,\dot{y}) - \widetilde{\mathcal{Z}}(y,\dot{y})||_2}{||\mathcal{Z}(y,\dot{y})||_2}\,\% \tag{33}$$

where $\widetilde{\mathcal{Z}}(y,\dot{y})$ is the hysteretic restoring force described by the Taylor series expansion.

The error analysis provides a convergence criterion for selecting the order of the Taylor series approach which can describe adequately the numerically integrated hysteresis loop, considering different excitation amplitudes for a quasi-static harmonic input $u(t) = A\sin(2\pi t)$ and varying the number of terms n. From Fig. 3, it can be concluded that upper than $n = 4$ terms the Taylor series expansion reaches the convergence, with the NMSE values above 2.5%. Fig. 4 shows a direct comparison between the hysteretic restoring force numerically integrated, and the paths $\mathcal{Z}_1, \mathcal{Z}_2, \mathcal{Z}_3$ and $\mathcal{Z}_4$ expanded using $n = 4$ terms in the Taylor series approach for the input amplitude of $A = 160$ N.

As observed, four terms in the Taylor series are enough to approach the hysteresis loop of the model benchmark properly under a high level of excitation amplitude, providing a close match within the responses and enclosing the same area of the hysteresis loop obtained by numerical integration, which is ≈ 83.1 mJ per cycle. Although $n = 4$ terms provide reasonable results, it is necessary to point out that n may change according to the shape of the hysteretic curve, having in mind that the higher the complexity in a hysteresis curve, the more terms need to be included. Having defined the framework of the piecewise hysteretic restoring force, the next step is to propose trial responses and later to compute the coefficients of the Fourier series using the Newton–Raphson method.

The frequency response curves obtained analytically and through numerical integration are shown in Fig. 5. The curves were estimated with a constant amplitude input $A = 10$ N over a normalized frequency range $\frac{\omega}{\omega_n} \in [0.11.8]$, examining as trial solutions for applying the harmonic balance method the fundamental harmonic ($\kappa = 1$) and the sum of the fundamental plus the third harmonic ($\kappa = 3$). The resonance frequency shifts up due to the hardening characteristic of the hysteretic restoring force, with the analytical responses capturing the jump phenomena between different amplitude solutions. Around the jump

[1] https://wxmaxima-developers.github.io/wxmaxima/

Table 1
Bouc-Wen model parameters proposed by Noël and Shoukens (2016) [46].

m [kg]	c [Ns/m]	k [N/m]	α [N/m]	β	γ [m^{-1}]	δ [m^{-1}]	ν
2	10	5×10^4	5×10^4	1×10^3	0.8	-1.1	1

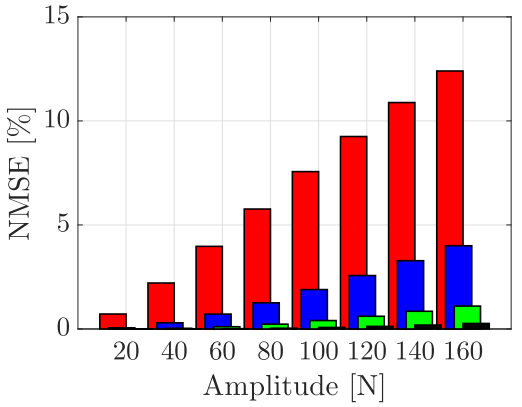

Fig. 3. Comparative error between different numbers of terms used in the Taylor series for approaching the hysteresis loop of the Bouc-Wen model. ■ represents $n = 2$ terms, ■ represents $n = 3$ terms, ■ represents $n = 4$ terms and ■ represents $n = 5$ terms.

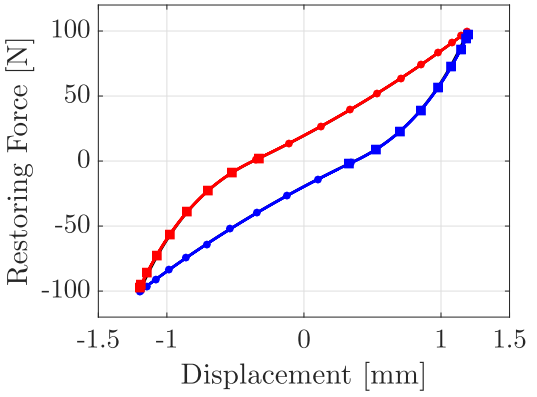

Fig. 4. Comparison between the hysteretic restoring forces of the Bouc-Wen model obtained from numerical integration of Eqs. 1,2 and through the four different paths approached by the Taylor series. ▬ is the $\mathcal{Z}(y, \dot{y})$ term response by numerical integration, whereas —■— represents $\mathcal{Z}_1$, —●— represents $\mathcal{Z}_2$, —■— represents $\mathcal{Z}_3$ and —●— is $\mathcal{Z}_4$.

resonant region, $\frac{\omega}{\omega_n} \in [1.1251.25]$, the choice of the initial conditions for estimating the coefficients of the harmonic components by the Newton–Raphson method require to be handled carefully. Moreover, the trial solution regarding the fundamental and third harmonic can predict well the subharmonic at frequency $\omega = \frac{\omega_n}{3}$, whereas only the fundamental harmonic cannot, as observed in Fig. 5(b).

Fig. 6 presents the normalized mean square error between the integrated numerical solution and the analytical responses for all the frequency interval. The error decreases on almost all the frequency spectrum for using the fundamental and the third harmonic as a trial solution, whereas only the first harmonic deviates from that calculated by the numerical integration. Also, the error achieves maximum values around the jump region, because the integrated numerical solution does not reproduce the jump effect.

Fig. 7 shows the hysteresis loop for different forcing conditions to assess the accuracy of the analytical solution with the fundamental and the third harmonic in predicting the Bouc-Wen response. It was considered three levels of amplitude 10, 20 and 40 N, applied for two different excitation frequencies of $\omega = \frac{\omega_n}{3}$ and $\omega = \omega_n$. The hysteresis loops predicted analytically through different amplitudes at $\omega = \frac{\omega_n}{3}$ shown in the Figs. 7(a), 7(c) 7(e) present substantially the same enclosed area, for instance, the dissipated energy from both the hysteresis loops in Fig. 7(e) is ≈ 3.35 mJ per period of oscillation. Figs. 7(b), 7(d) 7(f) show the comparison between both analytical and numerical loops when the excitation frequency is at $\omega = \omega_n$. For all cases with this excitation frequency, the area contained by the analytic hysteresis loop is smaller, for instance, in

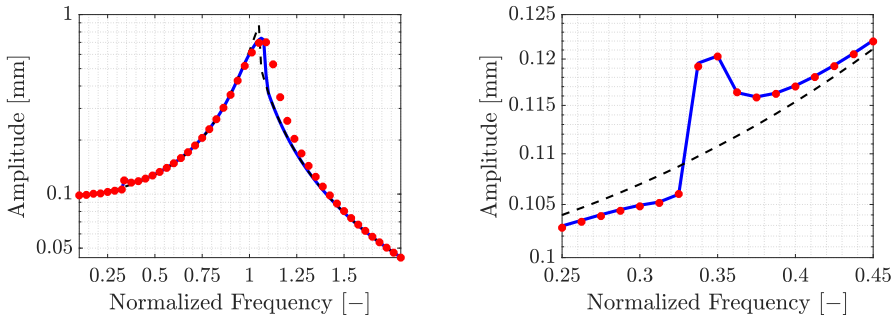

(a) Frequency response curve. (b) Zoom in the subharmonic $\omega = \frac{\omega_n}{3}$.

Fig. 5. Comparison between the frequency response curves of the Bouc-Wen model obtained with numerical integration and through harmonic balance method considering an input level of 10 N. · · · is the numerical integrated response, whereas – is the fundamental harmonic and ▬ is the fundamental added to the third harmonic.

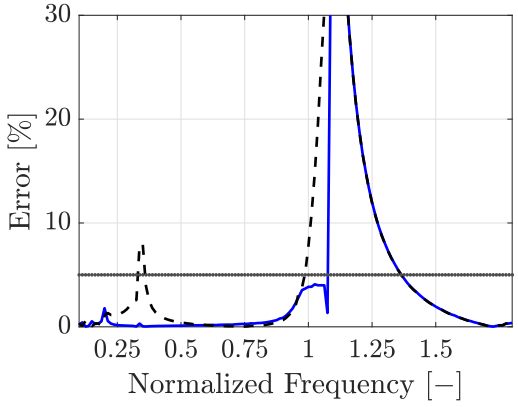

Fig. 6. Normalized mean square error between the numerical integrated solution and the analytical responses. – is the error between the fundamental harmonic and the numerical integrated curve, whereas ▬ is the error derived from the fundamental harmonic added to the third harmonic. The straight line ····· corresponds to the threshold error value of 5%.

Fig. 7(f) the analytic loop dissipates ≈ 72.4 mJ per period of oscillation, whereas the integrated numerical one corresponds to ≈ 87.9 mJ. Generally speaking, although there exist differences between the responses, the analytical solution is more conservative and, for this reason, it could help design purposes. Finally, Figs. 8 and 9 exemplify the responses in the time domain of the Figs. 7(e) and 7(f), respectively.

4.2. Numerical application for the LuGre model

The LuGre model parameters are addressed in Table 2. As performed for the Bouc-Wen application, the first step is to define the number of the terms that form the piecewise restoring forces from Eqs. (19) and (20). To achieve this purpose, a harmonic excitation $u(t) = A\sin(2\pi t)$ is considered, and the system output was also estimated by 4^{th} order Runge–Kutta method with variable time step.

Once again, the convergence analysis depicted in Fig. 10, which is based on the normalized mean square error between the numerically integrated hysteresis loop with regard the loop approached by the Taylor series, indicates that the NMSE remains above 2.5% for different input amplitudes when it is used upper than $n = 4$ terms. Fig. 11 displays a comparison among the hysteresis loop obtained by numerical integration and through $\mathcal{Z}_{\uparrow}(y)$ and $\mathcal{Z}_{\downarrow}(y)$ when approached by the Taylor series with $n = 4$ terms, evidencing a close match between the loops.

The fundamental added to the third harmonic are assumed as a trial response to compute the coefficients of the Fourier series for the friction model. Fig. 12 show the hysteresis loop of the LuGre model considering an amplitude of excitation $A = 1.2$ N and varying the excitation frequency in 0.1 and 1 Hz. For these forcing conditions, the response obtained by the harmonic balance method presents satisfactory agreement with the integrated numerical solution. The dissipated energy by both loops in Fig. 12(a) is ≈ 0.0125 mJ per period of oscillation, whereas in Fig. 12(b) the value is ≈ 0.0131 mJ.

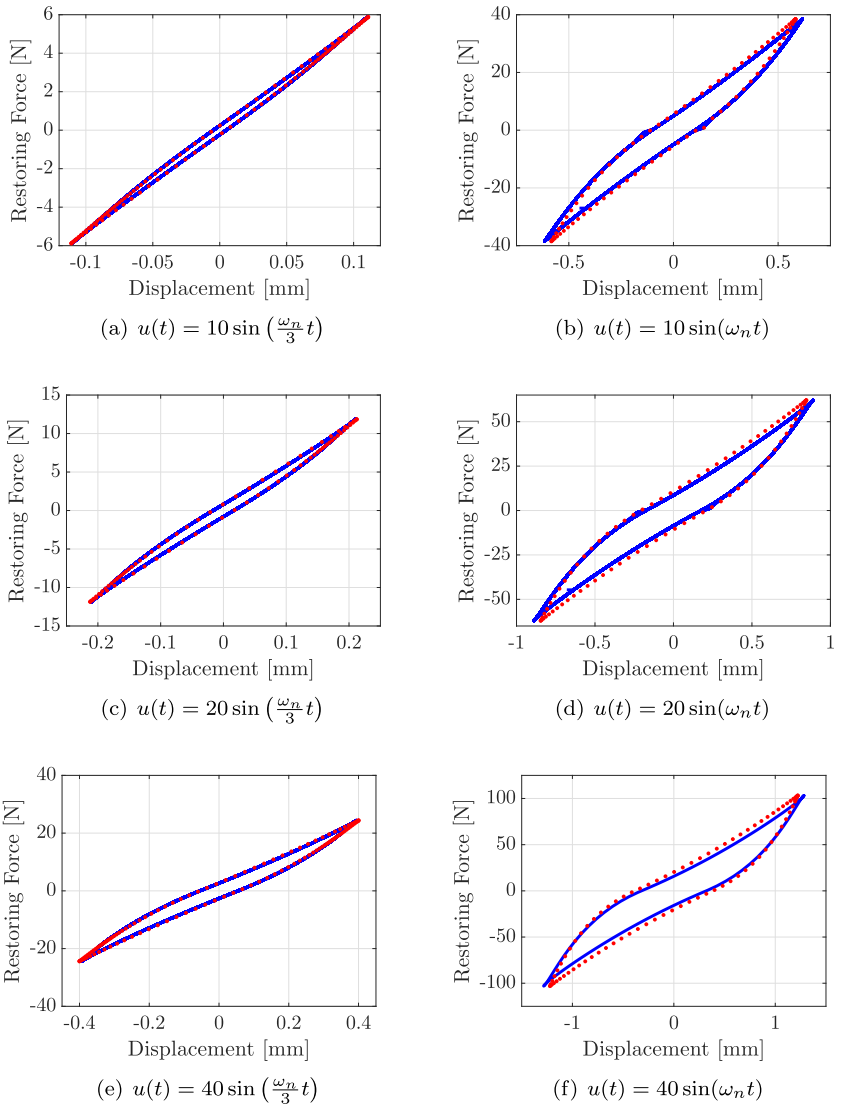

Fig. 7. Direct comparison between the hysteresis loop obtained by numerical integration and through the harmonic balance method considering different forcing conditions applied on the Bouc-Wen oscillator. ····· is the numerical integrated response, whereas ▬ corresponds to the analytical response.

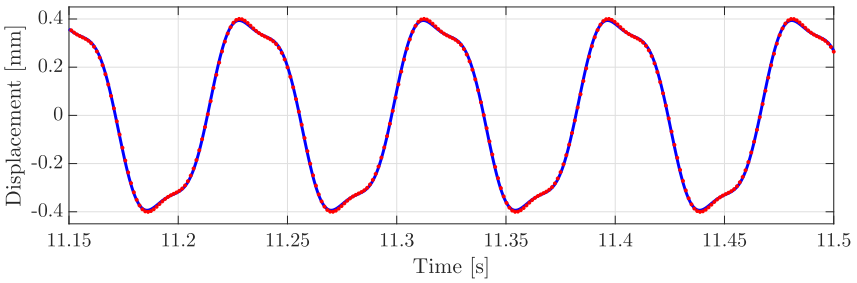

Fig. 8. Output identified by the harmonic balance method considering as input $u(t) = 40\sin\left(\frac{\omega_n}{3}t\right)$, in zoom between 11.15 and 11.5 seconds. ····· is the integrated numerical response, whereas ▬ corresponds to the analytical response.

Figs. 13 and 14 illustrate the time domain responses of Figs. 12 and 13, respectively. These two figures depict well one of the principal contributions proposed by this paper: the possibility of describing analytically the LuGre model operating in steady-state regime using few terms in the harmonic balance method and a much lower computational cost when compared with the numerical integration methods, since numerous periods are needed to reach the steady-state response.

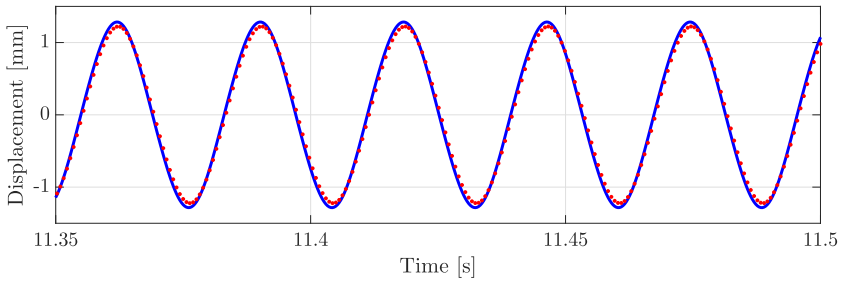

Fig. 9. Output identified by the harmonic balance method considering as input $u(t) = 40\sin(\omega_n t)$, in zoom between 11.15 and 11.5 seconds. ····· is the integrated numerical response, whereas ▬ corresponds to the analytical response.

Table 2
The LuGre model parameters proposed by Padthe et al. (2006) [20].

m [kg]	k [N/m]	σ_0 [N/m]	σ_1 [Ns/m]	c [Ns/m]	$\mathcal{F}_c$ [N]	$\mathcal{F}_s$ [N]	V_s[m/s]
1	2	10^5	$\sqrt{10^5}$	0.4	1	1.5	0.001

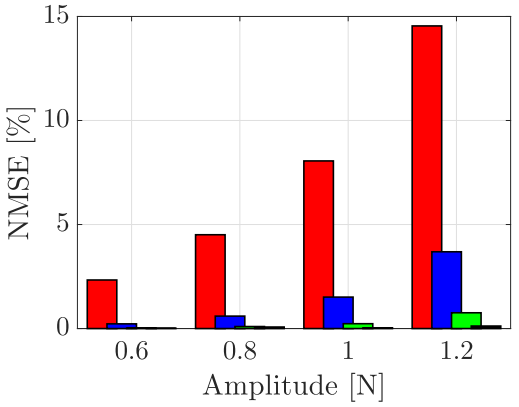

Fig. 10. Comparative error between different numbers of terms used in the Taylor series for approaching the hysteresis loop of the LuGre model. ■ represents $n = 2$ terms, ■ represents $n = 3$ terms, ■ represents $n = 4$ terms and ■ represents $n = 5$ terms.

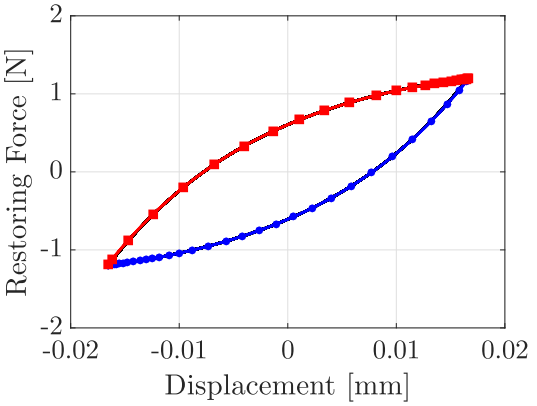

Fig. 11. Comparison between the hysteretic restoring forces obtained from numerical integration the LuGre model and through the loading and unloading regimes approached by the Taylor series. ▬ is the integrated numerical response; —■— represents $\mathcal{Z}_{\uparrow}(y)$ and —●— is $\mathcal{Z}_{\downarrow}(y)$.

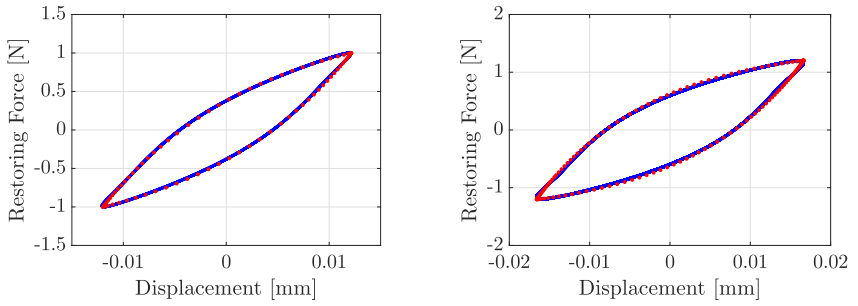

(a) Excitation frequency of $\omega = 0.2\pi$ (b) Excitation frequency of $\omega = 2\pi$

Fig. 12. Hysteresis loops of the LuGre model. ····· is the numerically integrated LuGre model response, whereas ▬ is the analytical solution.

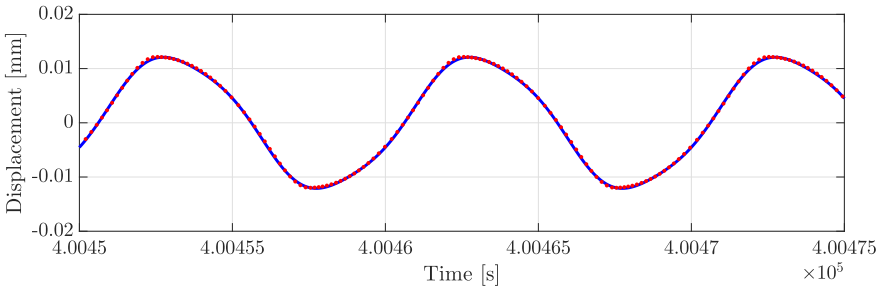

Fig. 13. Output in steady-state regime of the LuGre model identified by the harmonic balance method considering as input $u(t) = 1.2\sin(0.2\pi t)$, in zoom between 4.0045×10^5 and 4.0075×10^5 seconds. ····· is the numerically integrated LuGre model response, whereas ▬ is the analytical solution.

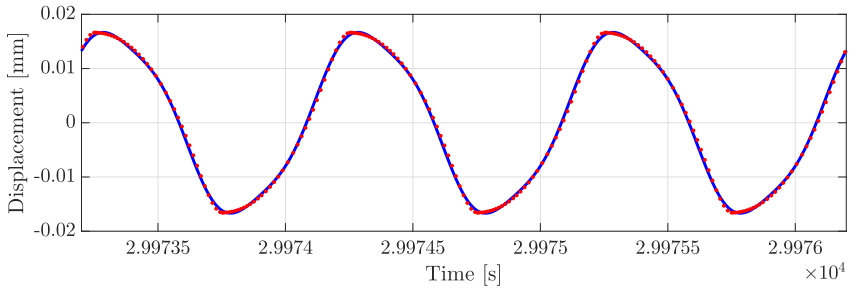

Fig. 14. Output in steady-state regime of the LuGre model identified by the harmonic balance method considering as input $u(t) = 1.2\sin(2\pi t)$, in zoom between 2.9973×10^4 and 2.9976×10^4 seconds. ····· is the numerically integrated LuGre model response, whereas ▬ is the analytical solution.

5. Final remarks

This work presents an analytical strategy of both the Bouc-Wen and LuGre hysteretic models through the harmonic balance method. The framework to rewrite the hysteretic restoring forces as piecewise smooth functions was performed using a simple Taylor series approach to expand them as explicit functions of the displacement. Further, the central particularities to use the harmonic balance method and then to determine balancing equations to calculate the coefficients of the Fourier series were discussed. As each piecewise expression is valid only at a specific frequency interval, the Fourier series has to be integrated by parts producing an average hysteretic restoring force based on splitting the coefficients of the series. A numerical application concerning the Bouc-Wen and the LuGre models, which are two challenging hysteretic models, was proposed to examine the accuracy of the proposed closed-form solutions. The harmonic balance method could predict the frequency response curve of the Bouc-Wen oscillator and to predict, excluding the jump resonant region, the hysteresis loop of the system. In the case of the LuGre model, the harmonic balance predicted with a close match the response of the friction model when subjected to a quasi-static harmonic input. Besides, the analytical solution could be an adequate alternative to obtain the steady-state response in a quick and practical step.

Although there exist criticism about the use of the harmonic balance method to describe analytically systems with hysteresis in the literature, this present paper proffered a new and simple way to approach the Bouc-Wen and LuGre models

using only the first three harmonics in the trial solution. In this way, this work opens up the possibility to propose, for future research, to extend the method for problems involving Finite Element based models and model updating with experimental data from practical engineering problems which present weak hysteresis. Also, expanding the algorithm of the harmonic balance method for systems with multiple-degrees-of-freedom, the methodology could be a welcome alternative to analyze the nonlinear normal modes of hysteretic systems. All these points can be addressed in further works.

Acknowledgments

The authors are thankful for the financial support provided by São Paulo Research Foundation (FAPESP) Grant No. 2016/21973–5, 2017/15512–8, 2018/14528–0, and Brazilian National Council for Scientific and Technological Development (CNPq) Grant No. 307520/2016–1. Additionally, the authors would like to thank the anonymous reviewers and the Associate Editor for their relevant comments and useful suggestions.

References

[1] Y. Song, C. Hartwigsen, D. McFarland, A. Vakakis, L. Bergman, Simulation of dynamics of beam structures with bolted joints using adjusted Iwan beam elements, J. Sound Vib. 273 (1) (2004) 249–276, https://doi.org/10.1016/S0022-460X(03)00499-1, URL: http://www.sciencedirect.com/science/article/pii/S0022460X03004991.
[2] F. Renaud, J.-L. Dion, G. Chevallier, I. Tawfiq, R. Lemaire, A new identification method of viscoelastic behavior: application to the generalized Maxwell model, Mech. Syst. Signal Process. 25 (3) (2011) 991–1010, https://doi.org/10.1016/j.ymssp.2010.09.002, URL: http://www.sciencedirect.com/science/article/pii/S0888327010003079.
[3] B.F. Spencer, S.J. Dyke, M.K. Sain, J.D. Carlson, Phenomenological model of a magnetorheological dampers, J. Eng. Mech. 123 (3) (1996) 230–238, URL: http://ascelibrary.org/doi/abs/10.1061/%28ASCE%290733-9399%281997%29123%3A3%28230%29.
[4] T. de P. Sales, D.A. Pereira, F.D. Marques, D.A. Rade, Modeling and dynamic characterization of nonlinear non-smooth aeroviscoelastic systems, Mechanical Systems and Signal Processing 116 (2019) 900–915.https://doi.org/10.1016/j.ymssp.2018.07.003. URL: http://www.sciencedirect.com/science/article/pii/S0888327018304035..
[5] M. Jokar, M. Ayati, A. Yousefi-Koma, H. Basaeri, Experiment-based hysteresis identification of a shape memory alloy-embedded morphing mechanism via stretched particle swarm optimization algorithm, J. Intell. Mater. Syst. Struct. 28 (19) (2017) 2781–2792, https://doi.org/10.1177/1045389X17698589.
[6] A. Visintin, Differential models of hysteresis, vol. 111, Springer Science & Business Media, 2013.
[7] R. Bouc, A mathematical model for hysteresis, Acta Acustica united with Acustica 24 (1) (1971) 16–25, URL: http://www.ingentaconnect.com/content/dav/aaua/1971/00000024/00000001/art00004.
[8] Y.-K. Wen, Method for random vibration of hysteretic systems, J. Eng. Mech. Div. 102 (2) (1976) 249–263.
[9] F. Ikhouane, J. Rodellar, Systems with hysteresis: analysis, identification and control using the Bouc-Wen model, John Wiley & Sons, 2007.
[10] Y. Shen, M.F. Golnaraghi, G.R. Heppler, Analytical and experimental study of the response of a suspension system with a magnetorheological damper, J. Intell. Mater. Syst. Struct. 16 (2) (2005) 135–147, https://doi.org/10.1177/1045389X05048330.
[11] D. Laxalde, F. Thouverez, J.-J. Sinou, Dynamics of a linear oscillator connected to a small strongly non-linear hysteretic absorber, Int. J. Non-Linear Mech. 41 (8) (2006) 969–978, https://doi.org/10.1016/j.ijnonlinmec.2006.09.002, URL: http://www.sciencedirect.com/science/article/pii/S0020746206000795.
[12] N. Okuizumi, K. Kimura, Multiple time scale analysis of hysteretic systems subjected to harmonic excitation, J. Sound Vib. 272 (3) (2004) 675–701, https://doi.org/10.1016/S0022-460X(03)00404-8, URL: http://www.sciencedirect.com/science/article/pii/S0022460X03004048.
[13] F. Ikhouane, J. Rodellar, On the hysteretic Bouc-Wen model, Nonlinear Dyn. 42 (1) (2005) 79–95, https://doi.org/10.1007/s11071-005-0070-x.
[14] K. Worden, C. Wong, U. Parlitz, A. Hornstein, D. Engster, T. Tjahjowidodo, F. Al-Bender, D. Rizos, S. Fassois, Identification of pre-sliding and sliding friction dynamics: grey-box and black-box models, Mech. Syst. Signal Process. 21 (1) (2007) 514–534, https://doi.org/10.1016/j.ymssp.2005.09.004, URL: http://www.sciencedirect.com/science/article/pii/S0888327005001408.
[15] S. Bograd, P. Reuss, A. Schmidt, L. Gaul, M. Mayer, Modeling the dynamics of mechanical joints, Mech. Syst. Signal Process. 25 (8) (2011) 2801–2826, https://doi.org/10.1016/j.ymssp.2011.01.010, URL: http://www.sciencedirect.com/science/article/pii/S0888327011000203.
[16] R. Lacayo, L. Pesaresi, J. Groß, D. Fochler, J. Armand, L. Salles, C. Schwingshackl, M. Allen, M. Brake, Nonlinear modeling of structures with bolted joints: A comparison of two approaches based on a time-domain and frequency-domain solver, Mech. Syst. Signal Process. 114 (2019) 413–438, https://doi.org/10.1016/j.ymssp.2018.05.033, URL: http://www.sciencedirect.com/science/article/pii/S0888327018302875.
[17] P. Niranjan, S. Karinka, K.V.S.S.S.S. Sairam, A. Upadhya, S. Shetty, Friction modeling in servo machines: a review, Int. J. Dyn. Control 6 (3) (2018) 893–906, https://doi.org/10.1007/s40435-017-0353-3.
[18] M. Vaishya, R. Singh, Sliding friction-induced non-linearity and parametric effects in gear dynamics, J. Sound Vib. 248 (4) (2001) 671–694, https://doi.org/10.1006/jsvi.2001.3818, URL: http://www.sciencedirect.com/science/article/pii/S0022460X01938180.
[19] C.C. de Wit, H. Olsson, K.J. Astrom, P. Lischinsky, A new model for control of systems with friction, IEEE Trans. Autom. Control 40 (3) (1995) 419–425, https://doi.org/10.1109/9.376053.
[20] A.K. Padthe, J. Oh, D.S. Bernstein, On the LuGre model and friction-induced hysteresis, in: American Control Conference, 2006, IEEE, 2006, pp. 6–pp. https://doi.org/10.1109/acc.2006.1657218..
[21] X.-R. Huang, L. Jézéquel, S. Besset, L. Li, O. Sauvage, Nonlinear modal synthesis for analyzing structures with a frictional interface using a generalized Masing model, J. Sound Vib. 434 (2018) 166–191, https://doi.org/10.1016/j.jsv.2018.07.027, URL: http://www.sciencedirect.com/science/article/pii/S0022460X18304711.
[22] M.F.M. Naser, F. Ikhouane, Hysteresis loop of the LuGre model, Automatica 59 (2015) 48–53, https://doi.org/10.1016/j.automatica.2015.06.006, URL: https://doi.org/10.1016%2Fj.automatica.2015.06.006.
[23] X. Jin, Y. Wang, Z. Huang, Approximately analytical technique for random response of LuGre friction system, Int. J. Non-Linear Mech. 104 (2018) 1–7, https://doi.org/10.1016/j.ijnonlinmec.2017.10.003, URL:http://www.sciencedirect.com/science/article/pii/S0020746217300872.
[24] C.W. Wong, Y.Q. Ni, S.L. Lau, Steady - state oscillation of hysteretic differential model. I: Response analysis, J. Eng. Mech. 120 (11) (1994) 2271–2298, https://doi.org/10.1061/(ASCE)0733-9399(1994)120:11(2271).
[25] Y. Ni, J. Ko, C. Wong, Identification of non-linear hysteretic isolators from periodic vibration tests, J. Sound Vib. 217 (4) (1998) 737–756, https://doi.org/10.1006/jsvi.1998.1804, URL: http://www.sciencedirect.com/science/article/pii/S0022460X98918041.
[26] V. Jaumouillé, J.-J. Sinou, B. Petitjean, An adaptive harmonic balance method for predicting the nonlinear dynamic responses of mechanical systems – application to bolted structures, J. Sound Vib. 329 (19) (2010) 4048–4067, https://doi.org/10.1016/j.jsv.2010.04.008, URL: http://www.sciencedirect.com/science/article/pii/S0022460X10002464.
[27] T.M. Cameron, J.H. Griffin, An alternating frequency/time domain method for calculating the steady-state response of nonlinear dynamic systems, J. Appl. Mech., ASME 56 (1) (1989) 149–154, https://doi.org/10.1115/1.3176036.

[28] D. Laxalde, F. Thouverez, Complex non-linear modal analysis for mechanical systems: application to turbomachinery bladings with friction interfaces, J. Sound Vib. 322 (4) (2009) 1009–1025, https://doi.org/10.1016/j.jsv.2008.11.044, URL: http://www.sciencedirect.com/science/article/pii/S0022460X08009528.
[29] S. Wang, L. Hua, C. Yang, X. Han, Z. Su, Applications of incremental harmonic balance method combined with equivalent piecewise linearization on vibrations of nonlinear stiffness systems, J. Sound Vib. 441 (2019) 111–125, https://doi.org/10.1016/j.jsv.2018.10.039, URL: http://www.sciencedirect.com/science/article/pii/S0022460X18307132.
[30] H. Jalali, An alternative linearization approach applicable to hysteretic systems, Commun. Nonlinear Sci. Numer. Simul. 19 (1) (2014) 245–257, https://doi.org/10.1016/j.cnsns.2013.05.020, URL: http://www.sciencedirect.com/science/article/pii/S1007570413002220.
[31] R.H. Hensen, M. Van de Molengraft, M. Steinbuch, Friction induced hunting limit cycles: a comparison between the LuGre and switch friction model, Automatica 39 (12) (2003) 2131–2137, https://doi.org/10.1016/s0005-1098(03)00234-6.
[32] P.R. Dahl, A solid friction model, Tech. rep. (may 1968).https://doi.org/10.21236/ada041920..
[33] K. Johanastrom, C. Canudas-de Wit, Revisiting the LuGre friction model, IEEE Control Syst. 28 (6) (2008) 101–114, https://doi.org/10.1109/mcs.2008.929425.
[34] S. da Silva, S. Cogan, E. Foltête, Nonlinear identification in structural dynamics based on Wiener series and Kautz filters, Mech. Syst. Signal Process. 24 (1) (2010) 52–58, https://doi.org/10.1016/j.ymssp.2009.05.017, URL: http://www.sciencedirect.com/science/article/pii/S0888327009001897.
[35] O. Scussel, S. da Silva, The harmonic probing method for output-only nonlinear mechanical systems, J. Braz. Soc. Mech. Sci. Eng. 39 (9) (2017) 3329–3341, https://doi.org/10.1007/s40430-017-0723-y.
[36] A. Nayfeh, Perturbation Methods, Physics textbook, Wiley, 2008, URL: http://books.google.com.br/books?id=eh6RmWZ51NIC.
[37] T. Kim, T. Rook, R. Singh, Super- and sub-harmonic response calculations for a torsional system with clearance nonlinearity using the harmonic balance method, J. Sound Vib. 281 (3) (2005) 965–993, https://doi.org/10.1016/j.jsv.2004.02.039, URL: http://www.sciencedirect.com/science/article/pii/S0022460X04002378.
[38] I. Kovacic, M. Brennan, The Duffing Equation: Nonlinear Oscillators and their Behaviour, John Wiley & Sons, 2011, URL: http://books.google.com.br/books?id=f6oZ0cwjTs8C.
[39] K. Worden, G.R. Tomlinson, Nonlinearity in structural dynamics, Institute of Physics Publishing (2001), https://doi.org/10.1201/9781420033823.
[40] S.d. Silva, S. Cogan, E. Foltête, F. Buffe, Metrics for nonlinear model updating in structural dynamics, J. Braz. Soc. Mech. Sci. Eng. 31 (1) (2009) 27–34, https://doi.org/10.1016/j.ijnonlinmec.2010.09.014.
[41] S. Bograd, P. Reuss, A. Schmidt, L. Gaul, M. Mayer, Modeling the dynamics of mechanical joints, Mech. Syst. Signal Process. 25 (8) (2011) 2801–2826, https://doi.org/10.1016/j.ymssp.2011.01.010, URL:https://doi.org/10.1016%2Fj.ymssp.2011.01.010.
[42] P. Bussetta, S.B. Shiki, S. da Silva, Nonlinear updating method: a review, J. Braz. Soc. Mech. Sci. Eng. 39 (11) (2017) 4757–4767, https://doi.org/10.1007/s40430-017-0905-7.
[43] L. Virgin, On the harmonic response of an oscillator with unsymmetric restoring force, J. Sound Vib. 126 (1) (1988) 157–165, https://doi.org/10.1016/0022-460x(88)90405-1.
[44] P. Donescu, L. Virgin, J. Wu, Periodic solutions of an unsymmetric oscillator including a comprehensive study of their stability characteristics, J. Sound Vib. 192 (5) (1996) 959–976, https://doi.org/10.1006/jsvi.1996.0228.
[45] W.-J. Kim, N. Perkins, Harmonic balance/Galerkin method for non-smooth dynamic systems, J. Sound Vib. 261 (2) (2003) 213–224, https://doi.org/10.1016/S0022-460X(02)00949-5, URL: http://www.sciencedirect.com/science/article/pii/S0022460X02009495.
[46] J. Noël, M. Schoukens, Hysteretic benchmark with a dynamic nonlinearity, in: Workshop on Nonlinear System Identification Benchmarks, Brussels, Belgium, 2016, pp. 7–14..
[47] J. Noël, A. Esfahani, G. Kerschen, J. Schoukens, A nonlinear state-space approach to hysteresis identification, Mech. Syst. Signal Process. 84 (Part B) (2017) 171–184, https://doi.org/10.1016/j.ymssp.2016.08.025, recent advances in nonlinear system identification URL: http://www.sciencedirect.com/science/article/pii/S0888327016303089.
[48] A.F. Esfahani, P. Dreesen, K. Tiels, J.-P. Noël, J. Schoukens, Parameter reduction in nonlinear state-space identification of hysteresis, Mech. Syst. Signal Process. 104 (2018) 884–895, https://doi.org/10.1016/j.ymssp.2017.10.017, URL: http://www.sciencedirect.com/science/article/pii/S0888327017305502.
[49] K. Worden, R. Barthorpe, E. Cross, N. Dervilis, G. Holmes, G. Manson, T. Rogers, On evolutionary system identification with applications to nonlinear benchmarks, Mech. Syst. Signal Process. 112 (2018) 194–232, https://doi.org/10.1016/j.ymssp.2018.04.001, URL: http://www.sciencedirect.com/science/article/pii/S0888327018301912.
[50] A. Bajrić, J. Høgsberg, Estimation of hysteretic damping of structures by stochastic subspace identification, Mech. Syst. Signal Process. 105 (2018) 36–50, https://doi.org/10.1016/j.ymssp.2017.11.042, URL: http://www.sciencedirect.com/science/article/pii/S0888327017306246.
[51] R.de O. Teloli, S. da Silva, A new way for harmonic probing of hysteretic systems through nonlinear smooth operators, Mech. Syst. and Signal Process. 121 (2019) 856–875, https://doi.org/10.1016/j.ymssp.2018.11.044, URL: http://www.sciencedirect.com/science/article/pii/S0888327018307659.
[52] R. Jiménez, L. Álvarez Icaza, LuGre friction model for a magnetorheological damper, Struct. Control Health Monitor. 12 (1) (2005) 91–116, https://doi.org/10.1002/stc.58, URL: https://onlinelibrary.wiley.com/doi/abs/10.1002/stc.58.
[53] L. Freidovich, A. Robertsson, A. Shiriaev, R. Johansson, LuGre-model-based friction compensation, IEEE Trans. Control Syst. Technol. 18 (1) (2010) 194–200, https://doi.org/10.1109/TCST.2008.2010501.
[54] J. Yao, W. Deng, Z. Jiao, Adaptive control of hydraulic actuators with LuGre model-based friction compensation, IEEE Trans. Industr. Electron. 62 (10) (2015) 6469–6477, https://doi.org/10.1109/TIE.2015.2423660.